

Gamma ray burst constraints on cosmological models from the improved Amati correlation

YANG LIU,¹ NAN LIANG,^{2,3} XIAOYAO XIE,^{2,3} ZUNLI YUAN,¹ HONGWEI YU,¹ AND PUXUN WU¹

¹*Department of Physics and Synergistic Innovation Center for Quantum Effects and Applications, Hunan Normal University, Changsha, Hunan 410081, China*

²*Key Laboratory of Information and Computing Science Guizhou Province, Guizhou Normal University, Guiyang, Guizhou 550025, China*

³*Joint Center for FAST Sciences Guizhou Normal University Node, Guiyang, Guizhou 550025, China*

(Received; Revised; Accepted)

Submitted to

ABSTRACT

An improved Amati correlation was constructed in (ApJ 931 (2022) 50) by us recently. In this paper, we further study constraints on the Λ CDM and w CDM models from the gamma ray bursts (GRBs) standardized with the standard and improved Amati correlations, respectively. By using the Pantheon type Ia supernova sample to calibrate the latest A220 GRB data set, the GRB Hubble diagram is obtained model-independently. We find that at the high redshift region ($z > 1.4$) the GRB distance modulus from the improved Amati correlation is larger apparently than that from the standard Amati one. The GRB data from the standard Amati correlation only give a lower bound limit on the present matter density parameter Ω_{m0} , while the GRBs from the improved Amati correlation constrain the Ω_{m0} with the 68% confidence level to be $0.308^{+0.066}_{-0.230}$ and $0.307^{+0.057}_{-0.290}$ in the Λ CDM and w CDM models, respectively, which are consistent very well with those given by other current popular observational data including BAO, CMB and so on. Once the $H(z)$ data are added in our analysis, the constraint on the Hubble constant H_0 can be achieved. We find that two different correlations provide slightly different H_0 results but the marginalized mean values seem to be close to that from the Planck 2018 CMB observations.

1. INTRODUCTION

Current observations, such as the type Ia supernovae (SN Ia) (Riess et al. 1998; Perlmutter et al. 1999), the cosmic microwave background radiation (CMB) (Spergel et al. 2003, 2007), and the baryon acoustic oscillation (BAO) (Eisenstein et al. 2005), indicate that the cosmic expansion is accelerating. To explain the origin of this peculiar phenomenon, commonly, a perfect fluid with negative pressure in the Universe dubbed dark energy is introduced. The nature of dark energy can be characterized by its equation of state (EoS) w . The simplest candidate of dark energy is the cosmological constant Λ , whose EoS is $w = -1$. The cosmological constant dark energy plus the cold dark matter make up the Λ CDM cosmological model, and the w CDM model is obtained if the EoS of dark energy is generalized from -1 to an arbitrary constant w . The simple Λ CDM model fits with observations (eBOSS Collaboration 2021) very well on one hand; however, on the other hand, it is plagued by the Hubble constant (H_0) tension (Perivolaropoulos & Skara 2021; Valentino et al. 2021). Based on the Λ CDM model, the high-redshift CMB data (Planck Collaboration 2020) give a tight constraint on H_0 ($67.4 \pm 0.5 \text{ km s}^{-1} \text{ Mpc}^{-1}$), which deviates from $H_0 = 73.2 \pm 1.3 \text{ km s}^{-1} \text{ Mpc}^{-1}$ given by the low-redshift SN Ia data (Riess et al. 2018a,b, 2021) more than 4σ . Although many other observations such as the Hubble parameter $H(z)$ measurements, the BAO, and the strong gravitational lenses have been used to discuss this H_0 tension, its origin is not yet determined (Wu et al. 2017; Chen et al. 2017; Abbott et al. 2018; Birrer et al. 2020;

yangl@hunnu.edu.cn

liangn@bnu.edu.cn

xyx@gznu.edu.cn

hwyu@hunnu.edu.cn

pxwu@hunnu.edu.cn

Cao et al. 2021a; Lin & Ishak 2021; Khetan et al. 2021; Efstathiou 2020; Freedman 2021; Cao & Ratra 2022b). Since the farthest redshift of the popular SN Ia, $H(z)$ and BAO data is about 2, while the CMB data lie near the redshift of 1100, the cosmological data during the region of middle redshift ($2 \lesssim z \lesssim 1100$) may play an important role in understanding the origin of the H_0 tension.

Gamma ray bursts (GRBs) are extremely energetic and thus detectable at a redshift up to $z \sim 9.4$ (Cucchiara et al. 2011). This implies that the GRBs have potential to serve as a new cosmological probe to the cosmic evolution in the middle redshift region. To standardize the GRBs and then use them to constrain the cosmological models, many empirical correlations between parameters of the light curves and/or spectra with the GRB luminosity or energy have been proposed (Norris et al. 2000; Fenimore & Ramirez-Ruiz 2000; Amati et al. 2002; Yonetoku et al. 2004; Ghirlanda et al. 2004a; Liang & Zhang 2005; Firmani et al. 2006; Dainotti et al. 2008, 2016; Demianski et al. 2017a; Wang et al. 2017, 2022; Hu et al. 2021; Luongo & Muccino 2021; Muccino et al. 2021; Cao et al. 2022c; Dainotti et al. 2022). However, to calibrate GRB correlations, a cosmological model is usually applied and the resulting correlations are later used to probe the cosmic evolution. Thus the GRB cosmology suffers the so called *circularity* problem (Ghirlanda et al. 2006; Wang et al. 2015). To avoid this problem, two different methods have been proposed. The first one is the *simultaneous fitting* or *global fitting* method (Ghirlanda et al. 2004b; Li et al. 2008), in which the coefficients of the correlations and the parameters of a cosmological model are constrained simultaneously from the GRB observations. The second one is the *low-redshift calibration* (Liang et al. 2008, 2010; Kodama et al. 2008; Wei & Zhang 2009), which bases on the idea of distance ladder, as the GRB correlations are calibrated by using other low redshift observations such as the $H(z)$ data (Amati et al. 2019; Montiel et al. 2021) or the SN Ia data (Demianski et al. 2017a,b, 2021). Up to now, the GRB data have been used widely to explore the components of our Universe, the nature of dark energy, and the Hubble constant tension (Demianski et al. 2017a,b, 2021; Liu & Wei 2015; Wang et al. 2016; Lin et al. 2016; Amati et al. 2019; Khadka & Ratra 2020; Cao et al. 2021b, 2022a).

Among the GRB empirical correlations, the Amati correlation is a very popular one, which connects the spectral peak energy in the GRB cosmological rest-frame and the isotropic equivalent radiated energy ($E_p - E_{\text{iso}}$) (Amati et al. 2002; Amati 2006a,b; Amati et al. 2008, 2009; Amati & Della 2013). Recently, we proposed an improved Amati correlation (Liu et al. 2022) by using the Gaussian *copula* which is a powerful statistical tool capable of describing the dependence structures between multivariate random variables, and has been applied to various fields by the astronomical community (Benabed et al. 2009; Koen 2009; Jiang et al. 2009; Scherrer et al. 2010; Takeuchi 2010; Yuan et al. 2018; Qin et al. 2020; Takeuchi & Kono 2020). In (Liu et al. 2022), by choosing the spatially flat Λ CDM model with $\Omega_{\text{m}0} = 0.30$ and $H_0 = 70 \text{ km s}^{-1} \text{ Mpc}^{-1}$ as the fiducial model, we utilize the low-redshift ($z < 1.4$) GRB data to calibrate the standard and improved Amati correlations, and then extrapolate the results to the high-redshift GRB data to achieve the GRB Hubble diagram, where $\Omega_{\text{m}0}$ is the present dimensionless matter density parameter. Using these calibrated GRBs to constrain the flat Λ CDM model, we found that the improved Amati correlation can give results well consistent with the fiducial model, while the standard one can not. Thus, in (Liu et al. 2022), the reliability of the improved Amati correlation was ascertained with a fiducial model, but its cosmological application was not carried out. In this work, we will fill this gap. In order to obtain the Hubble diagram of the latest A220 GRB samples (Khadka et al. 2021) model-independently, we use the Pantheon SN Ia data (Scolnic et al. 2018) to calibrate the standard and improved Amati correlations, and then use these calibrated GRB data to constrain the Λ CDM and w CDM models. Besides the GRB data, the $H(z)$ data set is also added in our analysis to obtain a tight constraint on model parameters.

The rest of the paper is organized as follows: Section 2 introduces the improved Amati correlation briefly, and standardizes the GRB samples by using the method of the low-redshift calibration. Section 3 studies the constraints on the Λ CDM and w CDM models from the GRB data and the GRB + $H(z)$ data. Our conclusions are summarized in Section 4.

2. GRB HUBBLE DIAGRAM FROM LOW-REDSHIFT CALIBRATION

2.1. Improved and standard Amati correlations

The standard Amati correlation is proposed by Amati et al. (2002), which describes a correlation between the spectral peak energy E_p and the isotropic equivalent radiated energy E_{iso} and has the form

$$y_{\text{Amati}} = a + bx \quad (1)$$

with

$$y \equiv \log \frac{E_{\text{iso}}}{1\text{erg}}, \quad x \equiv \log \frac{E_p}{300\text{keV}}. \quad (2)$$

Here “log” denotes the logarithm to the base of 10, and a and b are free coefficients. The spectral peak energy E_p and the isotropic equivalent radiated energy E_{iso} in Eq. (2) can be obtained through

$$E_p = E_p^{\text{obs}}(1+z), \quad (3)$$

$$E_{\text{iso}} = 4\pi d_L^2(z) S_{\text{bolo}}(1+z)^{-1}, \quad (4)$$

when the luminosity distance $d_L(z)$ is known. Here E_p^{obs} is the observed peak energy of the GRB spectrum, and S_{bolo} is the bolometric fluence, which is an observable.

The improved Amati correlation is derived from the *copula* function (Liu et al. 2022). To construct the correlation between x and y from the Gaussian *copula*, x and y are assumed to obey the Gaussian distributions, which are represented as $f(x)$ and $g(y)$, respectively. In addition, the GRB is assumed to obey a special redshift distribution $w(z) = ze^{-z}$ (Wang et al. 2017). Then, we use $F(x)$, $G(y)$ and $W(z)$ to indicate the cumulative distribution functions of $f(x)$, $g(y)$ and $w(z)$, respectively. According to the Sklar’s theorem (Nelson 2006), a joint distribution function \bar{H} can be constructed by using the Gaussian *copula* C :

$$\bar{H}(x, y, z; \boldsymbol{\theta}) = C(F(x), G(y), W(z); \boldsymbol{\theta}). \quad (5)$$

Here $\boldsymbol{\theta}$ denotes the parameters of the *copula* function. From the density function of the joint distribution, we obtain the improved Amati correlation, which takes the form (Liu et al. 2022)

$$y_{\text{copula}} = a + bx + c \operatorname{erfc}^{-1}[2W(z)]. \quad (6)$$

Here erfc^{-1} is the inverse of complementary error function and $W(z) = 1 - e^{-z}(1+z)$. Clearly, the improved Amati correlation has an extra redshift-dependent term compared with the standard one given in Eq. (1). When the coefficient c is fixed to be zero, the improved Amati correlation reduces to the standard one.

2.2. low-redshift calibration and GRB Hubble diagram

Eq. (4) indicates that to obtain the coefficients in the correlations from observations the luminosity distance needs to be given. In (Liu et al. 2022), this distance is given from the Λ CDM model and thus the results are model-dependent. To achieve a model-independent GRB Hubble diagram, here we utilize the method of the low-redshift calibration, and derive the luminosity distance in Eq. (4) from the Pantheon SN Ia samples by using the idea that at the same redshift the GRB has the same luminosity distance as the SN Ia.

In our analysis, we consider the A220 data set, which consists of A118 and A102 data sets and contains 220 long GRBs spanning the redshift from 0.03 to 8.2 (Khadka et al. 2021; Wang et al. 2016; Fana Dirirsa et al. 2019; Demianski et al. 2017a; Amati et al. 2019). This GRB data set is divided into the low-redshift part ($z < 1.4$), which has 79 data points, and the high-redshift one. To determine the values of coefficients in Eqs. (1) and (6), we use the linear interpolation to estimate the luminosity distance of 79 low-redshift GRB data points by following the method given in Appendix E1 in Betoule et al. (2014) to bin the 1048 Pantheon SN Ia data points into 35 bins in the $\log z$ space (see Appendix A for details). The binned results and 79 low-redshift ($z < 1.4$) GRBs calibrated by SN Ia are shown in Fig. 1. We must point out here that although the redshift of Pantheon SN Ia spans to $z = 2.26$, only the luminosity distances at $z \leq 1.4$ are used to calibrate the GRB. This is because there are only 6 SN Ia data points at $z > 1.4$, which is too few to estimate the luminosity distance accurately.

With the improved Amati correlation as an example, the values of coefficients (a , b , c) in Eq. (6) can be obtained from the 79 low-redshift GRBs by maximizing the D’Agostinis likelihood (D’Agostini 2005):

$$\mathcal{L}(\sigma_{\text{int}}, a, b, c) \propto \prod_i \frac{1}{\sqrt{\sigma_{\text{int}}^2 + \sigma_{y,i}^2 + b^2\sigma_{x,i}^2}} \times \exp \left[-\frac{[y_i - y_{\text{copula}}(x_i, z_i; a, b, c)]^2}{2(\sigma_{\text{int}}^2 + \sigma_{y,i}^2 + b^2\sigma_{x,i}^2)} \right], \quad (7)$$

where σ_x and σ_y are the uncertainties of x and y , respectively, and σ_{int} is the intrinsic uncertainty of GRBs. From the error propagation equation, we find that σ_y and σ_x can be derived from Eqs (3) and (4) as follows

$$\sigma_y = \frac{1}{\ln 10} \frac{\sigma_{E_{\text{iso}}}}{E_{\text{iso}}}, \quad \sigma_x = \frac{1}{\ln 10} \frac{\sigma_{E_p}}{E_p} \quad (8)$$

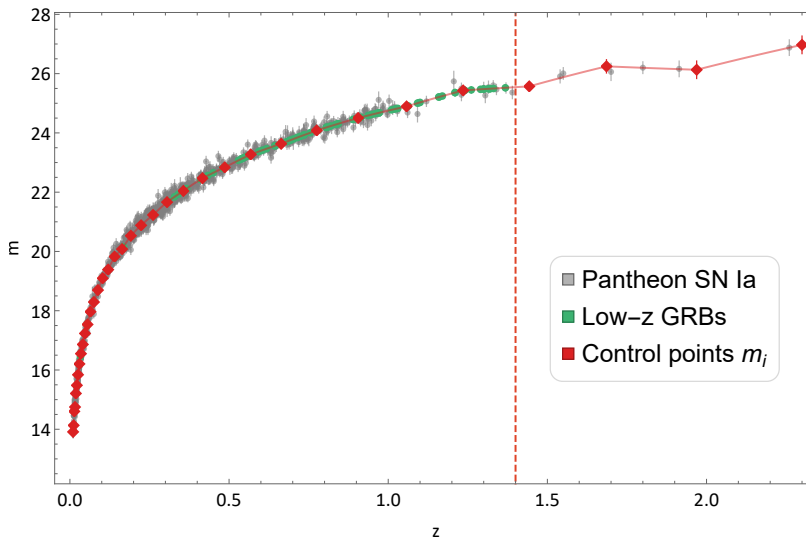


Figure 1. Apparent magnitudes of Pantheon SN Ia (gray points) and 36 log-spaced control points (red points). The green points are low-redshift ($z < 1.4$) GRBs calibrated by SN Ia. The red dashed line denotes $z = 1.4$.

Table 1. Constraints on the standard and improved Amati correlations from low-redshift calibration

Correlations	σ_{int}	a	b	c	$-2 \ln \mathcal{L}$
Standard Amati	0.511(0.047)	52.722(0.063)	1.295(0.135)	-	121.819
Improved Amati	0.509(0.045)	52.869(0.144)	1.194(0.149)	-0.232(0.206)	120.475

NOTE— The unmarginalized best-fitted values with standard deviations of standard and improved Amati correlations from 79 low-redshift GRBs.

with

$$\sigma_{E_{\text{iso}}} = 4\pi d_L^2 \sigma_{S_{\text{bolo}}} (1+z)^{-1}. \quad (9)$$

Here σ_{E_p} and $\sigma_{S_{\text{bolo}}}$ are available in the observations of GRBs. In our analysis, the *CosmoMC* code is used¹. The obtained values of σ_{int} and coefficients in Eqs. (1) and (6) are shown in Tab. 1. From it, one can see that the differences of σ_{int} and a between the standard and improved Amati correlations are negligible, while the difference of b is very significant. Furthermore, we find that the redshift-dependent correlation is favored since the value of c deviates from zero at the 1σ confidence level (CL).

Extrapolating the results from the low-redshift GRB data to the high-redshift one, one can derive the GRB luminosity distance from observations and obtain the corresponding distance modulus, which relates to the d_L through

$$\mu(z) = m - M = 25 + 5 \log \frac{d_L(z)}{\text{Mpc}}, \quad (10)$$

where m and M denote the apparent and absolute magnitudes, respectively. The uncertainty of the distance modulus is propagated from the uncertainties of S_{bolo} , E_{iso} and E_p :

$$\sigma_\mu^2 = \left(\frac{5}{2} \sigma_{\log \frac{E_{\text{iso}}}{\text{erg}}} \right)^2 + \left(\frac{5}{2 \ln 10} \frac{\sigma_{S_{\text{bolo}}}}{S_{\text{bolo}}} \right)^2, \quad (11)$$

¹ The *CosmoMC* code is available at <https://cosmologist.info/cosmomc>.

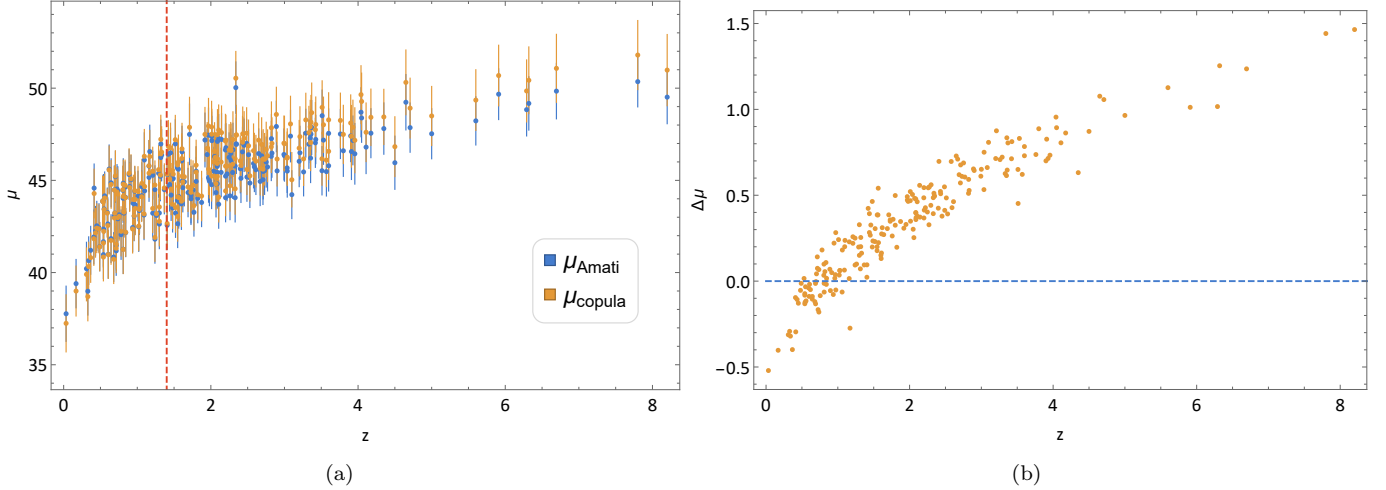


Figure 2. The left panel is the Hubble diagram of 220 long GRBs calibrated from the standard and improved Amati correlations (y_{Amati} and y_{copula}), respectively. The red dashed line denotes $z = 1.4$. The right panel shows the differences between μ_{copula} and μ_{Amati} ($\Delta\mu = \mu_{\text{copula}} - \mu_{\text{Amati}}$).

where

$$\begin{aligned} \sigma_{\log \frac{E_{\text{iso}}}{E_{\text{erg}}}}^2 &= \sigma_{\text{int}}^2 + \left(\frac{b}{\ln 10} \frac{\sigma_{E_p}}{E_p} \right)^2 + \sum_{i=1}^4 \left(\frac{\partial y_{\text{copula}}(x; \theta_c)}{\partial \theta_i} \right)^2 C_{ii} \\ &+ 2 \sum_{i=1}^4 \sum_{j=i+1}^4 \left(\frac{\partial y_{\text{copula}}(x; \theta_c)}{\partial \theta_i} \frac{\partial y_{\text{copula}}(x; \theta_c)}{\partial \theta_j} \right) C_{ij}. \end{aligned} \quad (12)$$

Here $\theta_c = \{\sigma_{\text{int}}, a, b, c\}$, and C_{ij} is the covariance matrix of these fitted coefficients. We construct the Hubble diagram of the GRBs and show it in Fig. (2a). The differences between μ_{copula} and μ_{Amati} are shown in Fig. (2b), which indicates that in the high-redshift region, the GRB distance modulus from the improved Amati correlation is larger apparently than that from the standard one.

3. CONSTRAINTS ON COSMOLOGICAL MODELS

The distance modulus of the A220 GRB data set can be used to constrain cosmological models by minimizing the χ^2 :

$$\chi_{\text{GRB}}^2 = \sum_{i=1}^N \left[\frac{\mu_{\text{GRB}}(z_i) - \mu_{\text{th}}(z_i; \mathbf{p}, \mu_0)}{\sigma_{\mu_i}} \right]^2, \quad (13)$$

where $N = 220$ is the number of the GRB data, $\mu_{\text{GRB}}(z_i)$ is the distance modulus of the GRB data at redshift z_i and μ_{th} denotes the theoretical value of the distance modulus, which is given by a cosmological model with \mathbf{p} representing the model parameters. In Eq. (13), $\mu_0 = 25 - 5 \log H_0$, which is a nuisance parameter and is marginalized here by using the analytical method given in (Nesseris & Perivolaropoulos 2004). Then, the χ_{GRB}^2 is modified to be

$$\tilde{\chi}_{\text{GRB}}^2 = A - \frac{B^2}{C}, \quad (14)$$

where

$$\begin{aligned} A &= \sum_{i=1}^N \left[\frac{\mu_{\text{GRB}}(z_i) - \mu_{\text{th}}(z_i; \mathbf{p}, \mu_0 = 0)}{\sigma_{\mu_i}} \right]^2, \\ B &= \sum_{i=1}^N \frac{\mu_{\text{GRB}}(z_i) - \mu_{\text{th}}(z_i; \mathbf{p}, \mu_0 = 0)}{(\sigma_{\mu_i})^2}, \\ C &= \sum_{i=1}^N \left(\frac{1}{\sigma_{\mu_i}} \right)^2. \end{aligned} \quad (15)$$

Except the GRB data, we also consider 31 Hubble parameter measurements (Stern et al. 2010; Moresco et al. 2012, 2016; Zhang et al. 2014; Moresco 2015; Ratsimbazafy et al. 2017; Ryan et al. 2018) spanning the redshift from 0.07 to 1.965, which are determined by the cosmic chronometric technique (Loeb 1998; Jimenez & Loeb 2002). For the $H(z)$ data set, the minimization of χ^2 method is also applicable:

$$\chi_{H(z)}^2 = \sum_{i=1}^N \left[\frac{H_{\text{obs}}(z_i) - H_{\text{th}}(z_i; \mathbf{p}, H_0)}{\sigma_{H_i}^{\text{obs}}} \right]^2. \quad (16)$$

Here $H_{\text{obs}}(z_i)$ is the Hubble parameter measurement at redshift z_i and H_{th} is the theoretical value of the Hubble parameter. The constraints on cosmological models from the GRB + $H(z)$ data can be obtained by minimizing

$$\chi_{\text{total}}^2 = \tilde{\chi}_{\text{GRB}}^2 + \chi_{H(z)}^2. \quad (17)$$

We consider two different cosmological models: Λ CDM and w CDM. The Hubble parameter $H(z)$ of the w CDM as a function of redshift z has the form

$$\frac{H(z; \mathbf{p})^2}{H_0^2} = E^2(z; \mathbf{p}) = \Omega_{\text{m}0}(1+z)^3 + (1 - \Omega_{\text{m}0})(1+z)^{3(1+w)}, \quad (18)$$

which reduces to that of the Λ CDM when $w = -1$. Thus, we have $\mathbf{p} \equiv \{\Omega_{\text{m}0}\}$ for the Λ CDM and $\mathbf{p} \equiv \{w, \Omega_{\text{m}0}\}$ for the w CDM. From Eq. (18), one can achieve the luminosity distance $d_L(z, \mathbf{p})$

$$d_L(z; \mathbf{p}) = \frac{(1+z)}{H_0} \int_0^z \frac{d\tilde{z}}{E(\tilde{z}; \mathbf{p})}. \quad (19)$$

The probability density distributions of the model parameters of two cosmological models are shown in Fig. (3), and the marginalized mean values with 68% CL of these parameters are summarized in Tab. 2. For a comparison, we consider both the standard and improved Amati correlations in standardizing the GRB. For the standard Amati correlation, it is easy to see that the GRB data only give a lower bound limit on the $\Omega_{\text{m}0}$, which is similar to the results obtained in (Khadka et al. 2021) with the simultaneous fitting method. While, the GRB data from the improved Amati correlation can constrain $\Omega_{\text{m}0}$ more effectively, and the mean values of $\Omega_{\text{m}0}$ are $0.308^{+0.066}_{-0.230}$ and $0.307^{+0.057}_{-0.290}$ in the Λ CDM and w CDM models, respectively. These results are consistent very well with those given by other current popular observation data including BAO, CMB and so on (Aubourg et al. 2015; Scolnic et al. 2018; Planck Collaboration 2020). Furthermore, we find that for the w CDM model the GRB data from the standard Amati correlation only give an upper bound limit on w at the 68% CL, but those from the improved Amati correlation can give a tighter constraint.

When the $H(z)$ data are added in our analysis, the GRB + $H(z)$ give tighter constraints $\Omega_{\text{m}0}$ and w than those from the GRB only. We find that the GRB data from improved Amati correlation always favors a smaller $\Omega_{\text{m}0}$ than that from the standard Amati correlation. The $H(z)$ +GRB from the improved Amati correlation can give a slightly tighter constraint on w than the $H(z)$ +GRB from the standard Amati correlation. We also investigate the limit on H_0 from the $H(z)$ +GRB. The results are shown in Fig. (4) and summarized in Tab. 2. It is easy to see that two different correlations provide slightly different constraints on the Hubble constant, but the marginalized mean values seem to be close to the one ($67.4 \pm 0.5 \text{ km s}^{-1} \text{ Mpc}^{-1}$) from the Planck 2018 CMB observations (Planck Collaboration 2020).

4. CONCLUSIONS

An improved Amati correlation was constructed from the Gaussian *copula* function recently by us (Liu et al. 2022). In this paper, we compare the constraints on cosmological models from GRB with the standard and improved Amati correlations. To obtain model-independently the GRB Hubble diagram, we use the Pantheon SN Ia data to calibrate the GRB data, and find that a redshift evolutionary correlation is favored slightly since the constant c , which is the coefficient of the redshift dependent term in the improved Amati correlation, deviates from the zero at the 1σ CL. The distance modulus of the GRB from the improved Amati correlation is apparently larger than that from the standard Amati correlation at the high-redshift region ($z > 1.4$). Thus, when the effect of the redshift evolution is neglected, the distance modulus of the GRBs will be underestimated at the high redshift region.

Using the GRBs to constrain the Λ CDM and w CDM models, we find that the data based on the standard Amati correlation only give a lower bound limit on $\Omega_{\text{m}0}$ and an upper bound one on w , while those from the improved Amati

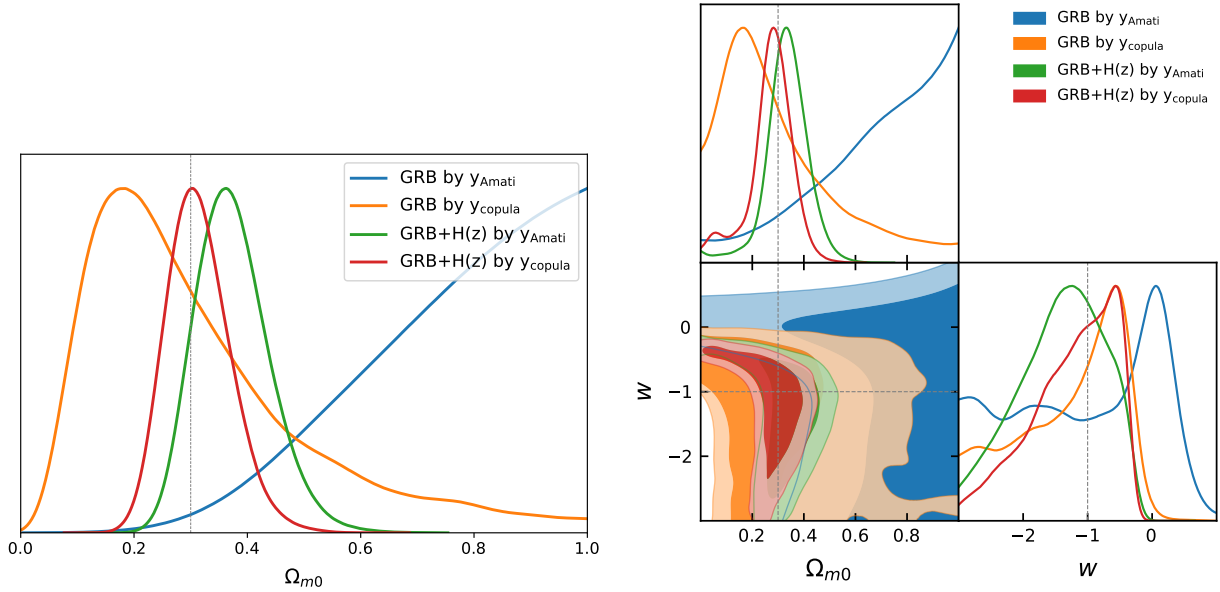


Figure 3. Constraints on the Λ CDM and the w CDM model from the GRB data and the GRB + $H(z)$ data.

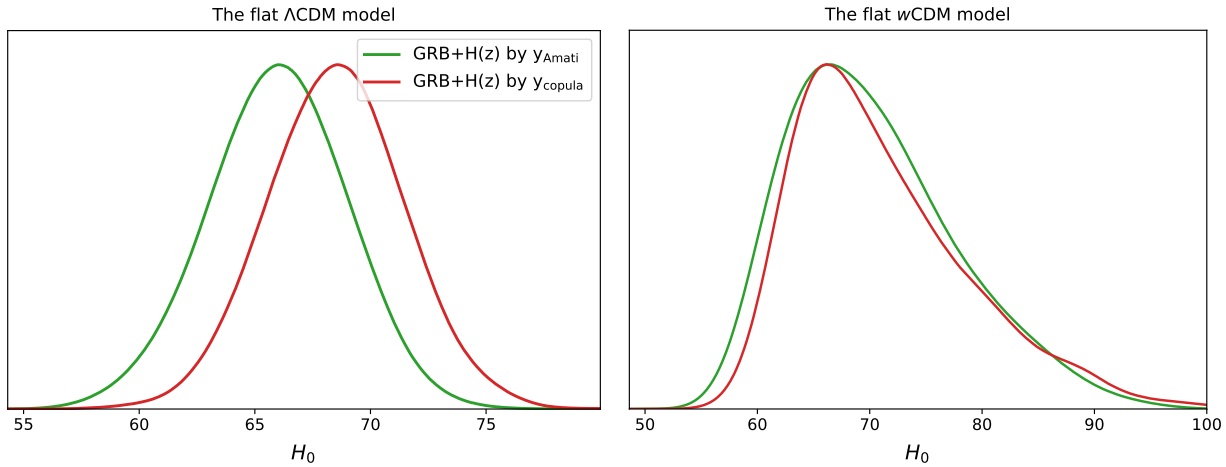


Figure 4. Constraints on H_0 from the GRB + $H(z)$ data. The green and red lines represent the results from the standard and improved Amati correlations, respectively.

correlation can constrain Ω_{m0} and w more tightly. The mean values of Ω_{m0} with the 68% CL are $0.308^{+0.066}_{-0.230}$ and $0.307^{+0.057}_{-0.290}$ in the Λ CDM and w CDM models, respectively, which are consistent very well with those given by other current popular observational data including BAO, CMB and so on (Aubourg et al. 2015; Scolnic et al. 2018; Planck Collaboration 2020). When the $H(z)$ data are added together to constrain Λ CDM and w CDM, tighter limits on Ω_{m0} and w are obtained. Furthermore, a constraint on H_0 is achieved. We find that two different correlations provide marginally different H_0 results but the marginalized mean values seem to be close to that from the Planck 2018 CMB observations (Planck Collaboration 2020).

ACKNOWLEDGMENTS

This work was supported in part by the NSFC under Grants No. 12075084, No. 11690034, No. 11805063, No. 11775077, and 12073069, by the Science and Technology Innovation Plan of Hunan province under Grant No. 2017XK2019, and by the Guizhou Provincial Science and Technology Foundation (QKHJC-ZK[2021] Key 020).

Table 2. Constraints on the Λ CDM and w CDM from the GRB data and the GRB + $H(z)$ data.

Correlations	Models	Data Sets	H_0	Ω_{m0}	w
y_{Amati}	Λ CDM	A220	-	> 0.651	-
		A220+ $H(z)$	$66.195(3.105)_{-3.139}^{+3.453}$	$0.370(0.067)_{-0.079}^{+0.050}$	-
	w CDM	A220	-	> 0.573	< -0.214
		A220+ $H(z)$	$70.176(7.701)_{-9.516}^{+5.161}$	$0.333(0.085)_{-0.068}^{+0.076}$	$-1.400(0.655)_{-0.496}^{+0.864}$
y_{copula}	Λ CDM	A220	-	$0.308(0.192)_{-0.230}^{+0.066}$	-
		A220+ $H(z)$	$68.543(2.954)_{-2.933}^{+2.861}$	$0.314(0.056)_{-0.063}^{+0.046}$	-
	w CDM	A220	-	$0.307(0.219)_{-0.290}^{+0.057}$	$-1.244(0.781)_{-0.463}^{+1.016}$
		A220+ $H(z)$	$70.857(7.644)_{-9.623}^{+4.310}$	$0.270(0.088)_{-0.052}^{+0.090}$	$-1.203(0.625)_{-0.327}^{+0.836}$

NOTE—The marginalized mean values, the standard deviations, and the 68% CL.

APPENDIX

A. BINNED DISTANCE MODULUS OF PANTHEON SN IA

Following the steps given in (Betoule et al. 2014), we use a piecewise linear function to approximate the apparent magnitudes m in the Pantheon SN Ia data, which is defined on each segment $z_i < z < z_{i+1}$ as

$$\bar{m}(z) = (1 - \alpha) m_i + \alpha m_{i+1} \quad (\text{A1})$$

with $\alpha = \log(z/z_i)/\log(z_{i+1}/z_i)$, where m_i is the apparent magnitude at z_i . For the 1048 Pantheon SN Ia data points, we segment 35 bins with 36 log-spaced control points in the redshift region $0.01 < z < 2.3$. To determine the value of m_i at each control point z_i , the minimizing χ^2 method is used:

$$\chi^2 = [\hat{\mathbf{m}}(z) - \bar{\mathbf{m}}(z)]^\dagger C^{-1} [\hat{\mathbf{m}}(z) - \bar{\mathbf{m}}(z)]. \quad (\text{A2})$$

Here C is the covariance matrix with 1048×1048 elements, and $\hat{\mathbf{m}}$ is a one-dimensional array with 1048 observations in the Pantheon SN Ia sample. The results of 36 log-spaced control points are shown in Tab. 3. Since only the apparent magnitudes are obtained, we will set the absolute magnitude to be $M = -19.36$ (Gómez-Valent 2022) in our analysis to obtain the luminosity distance of GRBs. If a different value of the absolute magnitude is chosen, it will change the value of coefficient a , but dose not affect the constraints on cosmological models.

REFERENCES

- Abbott, T. M. C., Abdalla, F. B., Annis, J., et al. 2018, *MNRAS*, 480, 3879
- Amati, L., Frontera, F., Tavani, M., et al. 2002, *A&A*, 390, 81
- Amati, L. 2006a, *NCimB*, 121, 1081
- Amati, L. 2006b, *MNRAS*, 372, 233
- Amati, L., Guidorzi, C., Frontera, F., et al. 2008, *MNRAS*, 391, 577
- Amati, L., & Della Valle, M. 2013, *Int. J. Mod. Phys. D*, 22, 1330028
- Amati, L., D’Agostino, R., Luongo, O., Muccino, M., & Tantaló, M. 2019, *MNRAS*, 486, L46
- Amati, L., Frontera, F., & Guidorzi, C. 2009, *A&A*, 508, 173
- Aubourg, É., Bailey, S., E. Bautista, J., et al. 2015, *PhRvD*, 92, 123516
- Benabed, K., Cardoso, J.-F., Prunet, S., & Hivon, E. 2009, *MNRAS*, 400, 219
- Betoule, M., Kessler, R., Guy, J., et al. 2014, *A&A*, 568, A22
- Birrer, S., Shajib, A. J., Galan, A., et al. 2020, *A&A*, 643, A165
- Cao, S., Ryan, J., & Ratra, B. 2021a, *MNRAS*, 504, 300

Table 3. Binned apparent magnitudes of the Pantheon SN Ia data.

z_i	m_i	σ_{m_i}	z_i	m_i	σ_{m_i}	z_i	m_i	σ_{m_i}
0.010	13.912	0.143	0.065	17.966	0.049	0.416	22.469	0.028
0.012	14.132	0.131	0.075	18.293	0.051	0.486	22.836	0.030
0.014	14.604	0.088	0.088	18.696	0.040	0.568	23.272	0.030
0.016	14.751	0.059	0.103	19.094	0.032	0.664	23.632	0.041
0.019	15.208	0.076	0.120	19.386	0.026	0.775	24.081	0.036
0.022	15.483	0.053	0.140	19.825	0.025	0.905	24.503	0.041
0.025	15.839	0.041	0.164	20.079	0.025	1.058	24.893	0.073
0.030	16.205	0.041	0.192	20.530	0.022	1.235	25.432	0.117
0.035	16.550	0.036	0.224	20.881	0.023	1.443	25.570	0.150
0.040	16.863	0.047	0.261	21.231	0.020	1.686	26.246	0.224
0.047	17.234	0.050	0.305	21.664	0.021	1.969	26.130	0.295
0.055	17.536	0.044	0.356	22.042	0.022	2.300	26.971	0.297

NOTE—The best-fitted value of binned apparent magnitude with standard deviation at each control point z_i .

- Cao, S., Ryan, J., Khadka, N., & Ratra, B. 2021b, *MNRAS*, 501, 1520
- Cao, S., Khadka, N., & Ratra, B. 2022a, *MNRAS*, 510, 2928
- Cao, S., & Ratra, B. 2022b, *MNRAS*, 513, 5686
- Cao, S., Dainotti, M., & Ratra, B. 2022c, *arXiv:2204.08710*
- Chen, Y., Kumar, S., & Ratra, B. 2017, *ApJ*, 835, 86
- Cucchiara, A., Levan, A. J., Fox, D. B., et al. 2011, *ApJ*, 736, 7
- Dainotti, M. G., Cardone V. F., & Capozziello S. 2008, *MNRAS Lett.*, 391, L79
- Dainotti, M. G., Postnikov, S., Hernandez, X., & Ostrowski, M. 2016, *ApJ*, 825, L20
- Dainotti, M. G., Nielson, V., Sarracino, G., et al. 2022, *arXiv:2203.15538*
- D’Agostini, G. 2005, *arXiv:physics/0511182*
- Demianski, M., Piedipalumbo, E., Sawant, D., & Amati, L. 2017a, *A&A*, 598, A112
- Demianski, M., Piedipalumbo, E., Sawant, D., & Amati, L. 2017b, *A&A*, 598, A113
- Demianski, M., Piedipalumbo, E., Sawant, D., & Amati, L. 2021, *MNRAS*, 506, 903
- eBOSS Collaboration. 2021, *PhRvD*, 103, 083533
- Efstathiou, G. 2020, *arXiv:2007.10716v2*
- Eisenstein, D. J., Zehavi, I., Hogg, D. W., et al. 2005, *ApJ*, 633, 560.
- Fana Dirirsa, F., Razzaque, S., Piron, F., et al. 2019, *ApJ*, 887, 13
- Femimore, E. E., & Ramirez-Ruiz, E. 2000, *arXiv:astro-ph/0004176*
- Firmani, C., Ghisellini, G., Avila-Reese, V., & Ghirlanda G. 2006, *MNRAS*, 370, 185
- Freedman, W. L. 2021, *ApJ*, 919, 16
- Gómez-Valent, A. 2022, *PhRvD*, 105, 043528
- Ghirlanda, G., Ghisellini, G., & Lazzati, D. 2004a, *ApJ*, 616, 331
- Ghirlanda, G., Ghisellini, G., Lazzati, D., & Firmani, C. 2004b, *ApJL*, 613, L13
- Ghirlanda, G., Ghisellini, G., & Firmani, C. 2006, *NewJ. Phys.*, 8, 123
- Hu, J. P., Wang, F. Y., & Dai, Z. G. 2021, *MNRAS*, 507, 730
- Jiang, I.-G., Yeh, L.-C., Chang, Y.-C., & Hung, W.-L. 2009, *AJ*, 137, 329
- Jimenez, R., & Loeb, A. 2002, *ApJ*, 573, 37
- Khadka, N., & Ratra, B. 2020, *MNRAS*, 499, 391
- Khadka, N., Luongo, O., Muccino, M., & Ratra, B. 2021, *JCAP*, 09, 042
- Khetan, N., Izzo, L., Branchesi, M., et al. 2021, *A&A*, 647, A72
- Kodama, Y., Yonetoku, D., Murakami, T., et al. 2008, *MNRAS*, 391, L1
- Koen, C. 2009, *MNRAS*, 393, 1370
- Li, H., Xia, J.-Q., Liu, J., et al. 2008, *ApJ*, 680, 92
- Liang, E., & Zhang, B. 2005, *ApJ*, 633, 611
- Liang, N., Xiao, W. K., Liu, Y., & Zhang, S. N. 2008, *ApJ*, 685, 354
- Liang, N., Wu, P., & Zhang, S. N. 2010, *PhRvD*, 81, 083518
- Lin, H.-N., Li, X., Chang, Z. 2016, *MNRAS*, 455, 2131
- Lin, W., & Ishak, M. 2021, *JCAP*, 05, 009
- Liu, J., & Wei, H. 2015, *Gen Relativ Gravit.*, 47, 141
- Liu, Y., Chen, F., Liang, N., et al. 2022, *ApJ*, 931, 50
- Loeb, A. 1998, *ApJ*, 499, L111

- Luongo, O., & Muccino, M. 2021, [arXiv:2110.14408](#)
- Montiel, A., Cabrera, J. I., & Hidalgo, J. C. 2021, *MNRAS*, 501, 3515
- Moresco, M. 2015, *MNRAS*, 450, L16
- Moresco, M., Cimatti, A., Jimenez, R., et al. 2012, *JCAP*, 08, 006
- Moresco, M., Pozzetti, L., Cimatti, A. et al. 2016, *JCAP*, 05, 014
- Muccino, M., Izzo, L., Luongo, O., et al. 2021, *ApJ*, 908, 181
- Nelson, R. B. 2006, *An Introduction to Copulas* (2nd ed.; New York: Springer)
- Nesseris, S., & Perivolaropoulos, L. 2004, *PhRvD*, 70, 043531
- Norris, J. P., Marani, G. F., & Bonnell, J. T. 2000, *ApJ*, 534, 248
- Perlmutter, S., Aldering, G., Goldhaber, G., et al. 1999, *ApJ*, 517, 565
- Perivolaropoulos, L., & Skara, F. 2021, [arXiv:2105.05208](#)
- Planck Collaboration. 2020, *A&A*, 641, A1
- Qin, J., Yu, Y., & Zhang, P. 2020, *ApJ*, 897, 105
- Ratsimbazafy, A. L., Loubser, S. I., Crawford, S. M., et al. 2017, *MNRAS*, 467, 3239
- Riess, A. G., Filippenko, A. V., Challis, P., et al. 1998, *AJ*, 116, 1009
- Riess, A. G., Rodney, S. A., Scolnic, D. M., et al. 2018a, *ApJ*, 853, 126
- Riess, A. G., Casertano, S., Yuan, W., et al. 2018b, *ApJ*, 861, 126
- Riess, A. G., Casertano, S., Yuan, W., et al. 2021, *ApJL*, 908, L6
- Ryan, J., Doshi, S., & Ratra, B. 2018, *MNRAS*, 480, 759
- Scherrer, R. J., Berlind, A. A., Mao, Q., & McBride, C. K. 2010, *ApJL*, 708, L9
- Scolnic, D. M., Jones, D. O., Rest, A., et al. 2018, *ApJ*, 859, 101
- Spergel, D. N., Verde, L., Peiris, H. V., et al. 2003, *ApJS*, 148, 175
- Spergel, D. N., Bean, R., Doré, O., et al. 2007, *ApJS*, 170, 377
- Stern D., Jimenez R., Verde L., Kamionkowski M., & Stanford S. A. 2010, *JCAP*, 02, 008
- Takeuchi, T. T., 2010, *MNRAS*, 406, 1830
- Takeuchi, T. T., & Kono, K. T. 2020, *MNRAS*, 498, 4365
- Valentino, E. D., Mena, O., Pan, S., Visinelli, L., Yang, W., Melchiorri, A., Mota, D. F., Riess, A. J., Silk, J., 2021, *Class. Quantum Grav.* 38, 153001
- Wang, F. Y., Dai, Z. G., & Liang, E. W. 2015, *New Astronomy Reviews*, 67, 1
- Wang, F. Y., Hu, J. P., Zhang, G. Q., & Dai, Z. G. 2022, *ApJ*, 924, 97
- Wang, G.-J., Yu, H., Li, Z.-X., Xia, J.-Q., & Zhu Z.-H. 2017, *ApJ*, 836, 103
- Wang, J. S., Wang, F. Y., Cheng, K. S., & Dai, Z. G. 2016, *A&A*, 585, A68
- Wei, H., Zhang, S. N. 2009, *EPJC*, 63, 139
- Wu, P.-X., Li, Z.-X., & Yu, H.-W. 2017, *FrP*, 12, 129801
- Yonetoku, D., Murakami, T., Nakamura, T., et al. 2004, *ApJ*, 609, 935
- Yuan, Z., Wang, J., Worrall, D. M., Zhang, B.-B., & Mao, J. 2018, *ApJS*, 239, 33
- Zhang, C., Zhang, H., Yuan, S., et al. 2014, *Res. Astron. Astrophys.*, 14, 1221